AGU PUBLICATIONS

Journal of Advances in Modeling Earth Systems

RESEARCH ARTICLE
10.1002/2016MS000629

# Radiative convective equilibrium as a framework for studying the interaction between convection and its large-scale environment

**Levi G. Silvers[1,2], Bjorn Stevens[1], Thorsten Mauritsen[1], and Marco Giorgetta[1]**

[1]The Max Planck Institute for Meteorology, Hamburg, Germany, [2]Now at Program in Atmosphere and Oceanic Sciences, Department of Geosciences, Princeton University/GFDL, Princeton, New Jersey, USA

**Key Points:**
- Radiative Convective Equilibrium (RCE) is a useful framework to compare, contrast, and harmonize the two extremes of explicit and parameterized convection
- Consistent climates across a range of domain sizes encourage the use of RCE to enhance our ability to model clouds (or cloud systems)
- The response of low clouds to warming, and hence estimation of the climate feedback parameter, is not robust across configurations

**Correspondence to:**
L. G. Silvers,
silvers@princeton.edu

**Citation:**
Silvers, L. G., B. Stevens, T. Mauritsen, and M. Giorgetta (2016), Radiative convective equilibrium as a framework for studying the interaction between convection and its large-scale environment, *J. Adv. Model. Earth Syst.*, *8*, 1330–1344, doi:10.1002/2016MS000629.

Received 7 JAN 2016
Accepted 21 JUL 2016
Accepted article online 25 JUL 2016
Published online 27 AUG 2016



**Abstract** An uncertain representation of convective clouds has emerged as one of the key barriers to our understanding of climate sensitivity. The large gap in resolved spatial scales between General Circulation Models (GCMs) and high resolution models has made a systematic study of convective clouds across model configurations difficult. It is shown here that the simulated atmosphere of a GCM in Radiative Convective Equilibrium (RCE) is sufficiently similar across a range of domain sizes to justify the use of RCE to study both a GCM and a high resolution model on the same domain with the goal of improved constraints on the parameterized clouds. Simulations of RCE with parameterized convection have been analyzed on domains with areas spanning more than two orders of magnitude ($0.80-204\times10^6 km^2$), all having the same grid spacing of 13 km. The simulated climates on different domains are qualitatively similar in their degree of convective organization, the precipitation rates, and the vertical structure of the clouds and water vapor, with the similarity increasing as the domain size increases. Sea surface temperature perturbation experiments are used to estimate the climate feedback parameter for the differently configured experiments, and the cloud radiative effect is computed to examine the role which clouds play in the response. Despite the similar climate states between the domains the feedback parameter varies by more than a factor of two; the hydrological sensitivity parameter is better behaved, varying by a factor of 1.4. The sensitivity of the climate feedback parameter to domain size is related foremost to a nonsystematic response of low-level clouds as well as an increasingly negative longwave feedback on larger domains.

## 1. Introduction

Research over at least the past two decades has shown that an uncertain representation of clouds, specifically tropical low-level clouds, is currently the largest source of spread among state-of-the-art climate models [*Cess et al*., 1989; *Bony and Dufresne*, 2005; *Stevens and Bony*, 2013]. Specific limitations of modeled clouds include both features which differ from what one observes (e.g., "too few, too bright," [*Webb et al*., 2001; *Nam et al*., 2012]) as well as features which are inadequately understood (e.g., controls on cloud vertical structure [*Nuijens et al*., 2015], and organization [*Bretherton et al*., 2005; *Muller and Held*, 2012; *Wing and Emanuel*, 2014]). An important component of these limitations is the delicacy of the interactions between clouds and circulations [*Bony et al*., 2015; *Sherwood et al*., 2014]. Efforts to better understand the role of moist convection in the climate system would be advanced by an ability to simulate the interaction between convection and the large-scale circulation using both models with parameterized convection and models with explicitly simulated convection. However, for these types of problems, making a logical and clear connection between Cloud Resolving Models (CRMs), and large-scale models that parameterize convection is difficult in large part because of the immensely differing range of parameters and large differences in the range of scales simulated, particularly for climate applications.

Global, or large-scale models using Radiative Convective Equilibrium (RCE) with parameterized convection have led to insights concerning tropical energetics of GCMs and the climate sensitivity [*Popke et al*., 2013; *Becker and Stevens*, 2014], and are increasingly being used to study the interplay between convection and large-scale circulations [*Arnold and Randall*, 2015]. It has also become clear that even with the relative simplicity of RCE, differences in convective parameterization schemes play a decisive role on the overall statistics of the simulation [*Popke et al*., 2013; *Coppin and Bony*, 2015; *Reed et al*. 2015]. Due to the multiplicity of

solutions that previous RCE simulations have produced [*Held et al*., 2007; *Jeevanjee and Romps*, 2013; *Emanuel et al*., 2014; *Wing and Cronin*, 2016; *Zhou*, 2015] which depend on domain details, grid-spacing, surface temperature, and parameterizations, we cannot per se assume that solutions of GCM-RCE simulations will be independent of domain size. Examining these domain size effects using simulations with parameterized convection, extending to near global scales, is the aim of this paper.

Although not specifically focused on details of the convection or cloud feedbacks, early studies of RCE [*Manabe and Strickler*, 1964; *Manabe and Wetherald*, 1967] led to fundamental advancements in our understanding of the atmosphere. The overall surface warming from high clouds and cooling from low clouds was first shown by Manabe and Strickler. Manabe and Wetherald showed the equilibrium surface temperature warming in RCE, for a specified change in atmospheric $CO_2$, is strongly dependent on whether atmospheric relative humidity or absolute humidity is assumed fixed as the surface is warmed. In the ensuing decades cloud resolving models have also been used to simulate RCE. So doing allowed assumptions about the structure of the atmosphere, convection, and clouds to be relaxed as more atmospheric processes could be resolved by the simulations. These pioneering studies have come back into focus with the realization that convective aggregation arises spontaneously from simulations with an explicit representation of convection [e.g., *Nakajima and Matsuno*, 1988; *Held et al*., 1993; *Tompkins and Craig*, 1998; *Bretherton et al*., 2005; *Muller and Held*, 2012], in ways that depend on temperature [*Wing and Emanuel*, 2014], thereby raising the question as to its importance for the climate system [*Bony et al*., 2015; *Mauritsen and Stevens*, 2015; *Coppin and Bony*, 2015].

Previous work has shown how fruitful the strategy of linking convection-resolving to parameterized convective models can be. For example the observational analysis by *Redelsperger et al*. [2002] highlighted a strong dependence of tropical convection on tropospheric humidity. Convective parameterizations were then shown by *Derbyshire et al*. [2004] not to reproduce this behavior as modeled by CRMs. Subsequently, the convection scheme in the European Center for Medium-Range Weather Forecasting (ECMWF) model was modified to include a dependence on relative humidity of the entrainment rate [*Bechtold et al*., 2008]. These changes led to significant improvements in the representation of the atmospheric variability in the ECMWF model. Simulations of the diurnal timing of precipitation have also benefited from comparisons between convection-resolving idealized models and global, highly parameterized models [*Rio et al*., 2009; *Bechtold et al*., 2014].

Despite these cases of cooperation between models using resolved and parameterized convection, a cleaner experimental configuration in which GCMs and CRMs could be compared would be useful. This paper explores the possibility of using RCE in this context. We analyze the features of an atmosphere with parameterized convection as a function of domain size to explore the applicability of such a configuration.

Simulations using parameterized physics and a coarse grid, commensurate to what one might use for a high-resolution GCM study, and with an explicit representation of convection on a necessarily fine grid are now feasible for domains on the order of $10^6$ km$^2$. This possibility naturally raises the question as to whether a direct comparison between GCMs and CRMs is likely to be influenced by the choice of the domain size, or whether there are robust features of the simulations that can be expected to emerge irrespective of a given domain size. The recently developed model ICON (ICOsahedral Nonhydrostatic) has the flexibility to allow simulations across a range of scales, thereby providing a unifying framework for studying convection at different scales and with different degrees of parameterization. All of the simulations presented in this paper use parameterized convection. In addition to simulations with a fixed SST on domains of different sizes (e.g., Figure 1) simulations are performed with fixed SSTs (297 K and 301 K) to test whether climate feedbacks are sensitive to domain size. As if not, this raises the possibility of using CRMs directly, on smaller domains, to constrain estimates of climate sensitivity.

Shown in Figure 1 is the total precipitation rate from simulations (described in the next section) using the ICON model with parameterized convection on five different domains. The only difference between these simulations is domain size, which is described throughout using the unit M (1M$=10^6$ km$^2$; Mega km$^2$). The domains range in size from slightly larger than Texas ($0.80\times10^6$ km$^2$; 3/4M), to almost half of the surface area of the Earth ($204\times10^6$ km$^2$; 200M). The precipitating structures organize on the scale of the domain, and show a slight tendency toward stronger precipitation and more organization as the domain size increases. These structures continuously evolve while moving through the domains. However, it will be

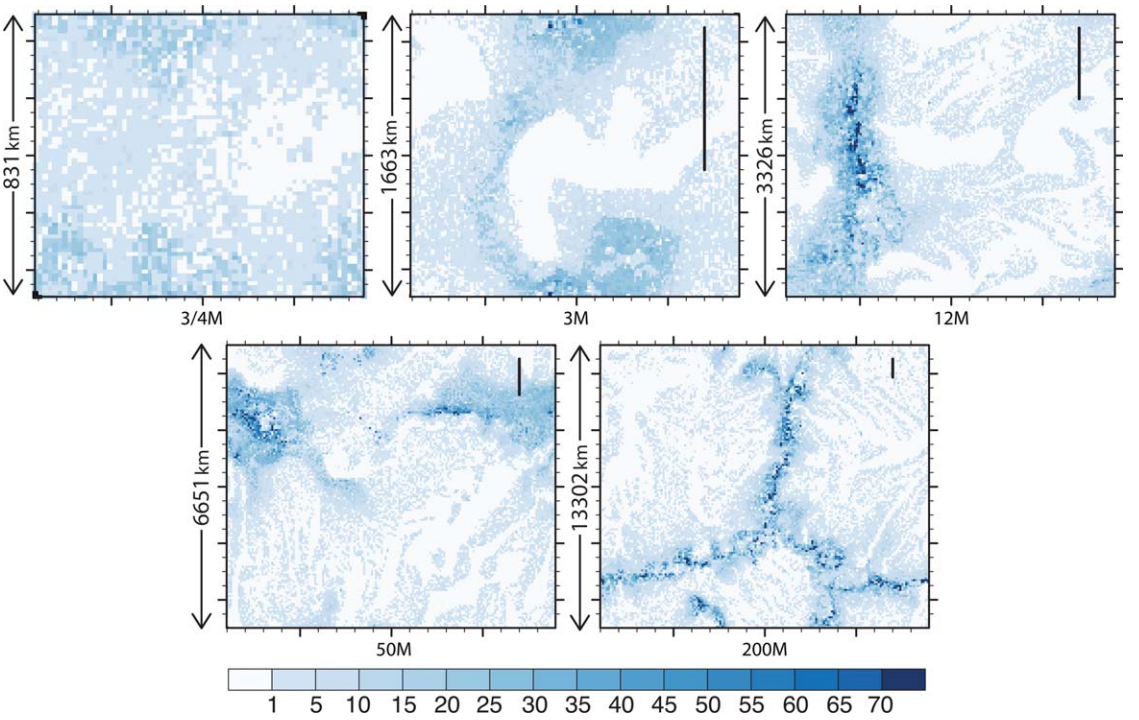


**Figure 1.** Precipitation rate (mm $d^{-1}$) of the equilibrated state for the five domains with a constant SST of 301 K. Domain sizes are labeled as 3/4M, 3 M, 12 M, 50M, 200M, with increasing numbers indicating a four-fold increase in area (see Table 1). For comparison, the black bar in the 3M, 12M, 50M, and 200M domains represents a length of 830 km, corresponding to the short edge length of the 3/4M domain.

shown that the solutions are quite similar when measured statistically, for instance in terms of the mean subsidence fraction and the mean vertical structure of the simulated atmosphere. To the extent that the simulated climates of these domains are similar there is reason to think that improved constraints of the parameterized convective response on a small domain, for instance through the application of cloud resolving models, would also improve the parameterized convection of a global simulation.

The design of the simulations and details of the model used are presented in the next section. In section 3 results are presented both in terms of the mean atmospheric state, and the response to a perturbation of 4 K to the SST. Section 3 also explores robust differences in the response to warming, and suggests that while many changes in the simulated atmosphere do not depend on domain size, the climate sensitivity is sensitive to small differences that are not robust across domains. Despite having the same core model and identical physics, the total radiative feedback from warming still varies by about a factor of two across domain sizes. Discussion and conclusions are given in section 4.

## 2. Experimental Design and Model Setup

### 2.1. Methodology

The framework of RCE is used here to focus on the interactions between radiation, large-scale circulation, and clouds without the complicating influence of heterogeneities imposed on the large scale. Despite homogeneous forcing, the spontaneous emergence of large-scale overturning circulations, as also emphasized by *Popke et al*. [2013], makes it possible to capture the interplay of clouds with these circulations, in contrast to single column model studies. Two simulations with constant SST values of 297 K and 301 K are made on five doubly periodic domains of different size but identical grid spacing. The Coriolis force is set to zero everywhere and the insolation and profiles of trace-gases (e.g., ozone) are made horizontally uniform. The cosine of the zenith angle is $\pi/4$ and the insolation used is 340.3 $Wm^{-2}$, approximately equal to Earth's global annual mean value. There is no diurnal cycle and a surface of water at a fixed temperature defines the lower boundary. One result of this is that neither the surface nor the top of the atmosphere is expected to have a balanced energy budget. However, the flux of energy into and out of the atmosphere will be

**Table 1.** Length of Simulations, SST Used, Size and Names of Domains for Each Simulation[a]

| Domain | Area ($km^2$) | Edge Length (km) | Grid Points | SST (K) | Length (year) | P1 (year) | P2 (month) |
|---|---|---|---|---|---|---|---|
| 3/4M | $0.80\times10^6$ | $960 \times 831$ | 4,608 | 297/301 | 10 | 9 | 12 |
| 3M | $3.2\times10^6$ | $1,920 \times 1,663$ | 18,432 | 297/301 | 10 | 9 | 4 |
| 12M | $12.8\times10^6$ | $3,840 \times 3,326$ | 73,728 | 297/301 | 4 | 3 | 8 |
| 50M | $51.1\times10^6$ | $7,680 \times 6,651$ | 294,912 | 297/301 | 2 | 1 | 4 |
| 200M | $204\times10^6$ | $15,360 \times 13,302$ | 1,179,648 | 297/301 | 1 | 0.6 | 0.76 |

[a]The M in the domain names stands for million (or Mega) $km^2$. Also shown are two different periods (P1 and P2) of time used for computing mean values from the end of the simulations. See text and figure captions for details.

balanced once the energy content of the atmosphere equilibrates with its forcing, which, after the initial adjustment period, remains steady in time except for weather related fluctuations. This provides a simple framework for analyzing the behavior of the convection and the sensitivity of the feedback processes yet retains the full complexity of the physics and dynamical equations.

We have computed simulations on five different domains, ranging from about the size of the global tropics (area $=204\times10^6 km^2$, side length $=15,360$ km) down to a regional scale of $\sim8\times8$ degrees (area $=0.80\times10^6 km^2$, side length $=960$ km); the lower bound on scale was chosen for feasibility of comparison with high-resolution models. In addition to varying the size of the domain, simulations with different SST values allow us to examine the climatic response to warming perturbations, and compute the total feedback that results from the warming.

Because there are fewer grid points on the smaller domains, the degree of variability in the domain mean per time step increases as the domain size decreases. This is because a given perturbation will have a larger influence on the statistics of a domain with fewer grid points, relative to a domain with more grid points. To obtain comparable statistics between the various domains, and take advantage of the computational economy of the smaller domains, the length of simulation increases as the domain size decreases. Details of the simulations examined in this paper are given in Table 1. The periods used for computing feedback and sensitivity parameters and cloud radiative effects (P1) and domain mean profiles (P2) are given in Table 1. The increased length of P1 was necessary to obtain robust statistics for the feedback parameters of the different domains.

### 2.2. Model Details

The horizontal grid used in this study consists of equilateral triangles on a plane with periodic boundary conditions in both dimensions. The ICON model solves the fully three-dimensional nonhydrostatic and compressible Navier-Stokes equations and is described in detail in *Zängl et al.* [2015]. All of the simulations described here use triangles with an edge length of 20 km, implying an effective grid spacing of about 13 km (defined as $\sqrt{\text{cell area}}$ in *Zängl et al.* [2015]). This grid spacing is chosen to match the operational resolution used by the German weather service (Deutsche Wetter Dienst: DWD). The vertical coordinate is a height-based hybrid coordinate with 60 vertical levels between the surface and the model top at 40 km. The top of the model uses a Rayleigh damping of the vertical wind following *Klemp et al.* [2008] to prevent the reflection of gravity waves from the model top. The variables are positioned on a regular-triangular C-grid with a combination of first- and second-order finite difference spatial discretizations. Time integration is computed with a two time-level predictor-corrector scheme with the physics parameterizations split into slow and fast modes. Further information on discretization aspects of triangular grids are discussed in *Gassmann* [2011] and *Wan et al.* [2013]. The ongoing development of ICON is a joint project between the Max Planck Institute for Meteorology (MPI-M) and DWD. Thus ICON has been developed as a unified modeling framework that functions both as an operational weather forecast model and a global climate model, albeit with a different set of parameterizations. ICON can also be used as a Large Eddy Simulation model capable of explicitly representing canonical cloudy boundary layer flows on grid meshes as fine as 50 m or less [*Dipankar et al.*, 2015].

The physics parameterizations used in the present study are the NWP physics, so named because they are used operationally by DWD in their global implementation of ICON. The cumulus convective parameterization is a bulk mass-flux scheme that allows deep, shallow, and midlevel convection [*Bechtold et al.*, 2001, 2008]. To close the system it is assumed that convective available potential energy is consumed by the

cumulus convection over a particular time scale. The radiative transfer scheme is an RRTM scheme similar to that used in the IFS model and identical to that of the ECHAM6.1 model [*Mlawer et al*., 1997; *Stevens et al*., 2013]. The microphysics scheme is from the COSMO-EU five-category prognostic scheme [*Seifert*, 2008] predicting rain, snow, cloud ice, cloud liquid water, and water vapor. Relative humidity is computed over a liquid surface only. The cloud cover scheme is based on a fixed width box-function probability density function of total water (similar to the parameterization of *Sundqvist* [1978]) with an added diagnostic anvil term that uses the detrainment from the convective parameterization. Thus a relative humidity threshold is defined beyond which cloud cover forms. The boundary layer and turbulence scheme relies on a prognostic equation for turbulent kinetic energy [*Raschendorfer*, 2001]. Interactions between the turbulence scheme and subgrid-scale clouds follow the statistical model of *Sommeria and Deardorff* [1977]. For these experiments gravity waves are not parameterized. The development of these schemes is ongoing, those used for this study correspond to revision number 16400. As an additional option to the NWP physics parameterizations used here, a successor to the ECHAM6 physics is also being implemented into ICON at MPI-M which will be used for climate studies.

The profile used for the ozone is representative of the tropics and is the same profile used by *Popke et al*. [2013]. To trigger the adjustment process, perturbations of 0.2 K, white in spatial distribution, were applied to the initial potential temperature field in the lowest four model levels. The initial values of the vertical, $w$, and one component, $v$, of the horizontal velocity fields are zero. In the lowest 2.5 km the horizontal velocity $u$ begins with an exponentially decaying profile (5 m s$^{-1}$ at the surface), which is dissipated to near zero within the first few hours of each experiment. For the simulations to behave reasonably it was necessary to specify a minimum surface wind velocity scale used only in the computation of the surface fluxes. This required adding 0.8 m s$^{-1}$ to the default value used in the physics (0.01 m s$^{-1}$). The initial profiles for potential temperature, and water vapor are idealized based upon the best fit to profiles from a large-eddy simulation. The potential temperature was initialized as $\theta=\theta_{sfc}+4.8z$ below the tropopause and as $\theta=\theta_{sfc}+4.8z_{tp}+22.0(z-z_{tp})$ at and above the tropopause, where $\theta$ is potential temperature (K), $z$ is height (km) and the subscripts 'tp' and 'sfc' represent the values at the tropopause level and surface, respectively. The water vapor was initialized as an exponentially decaying concentration with a scale height of 2.8 km and an initial surface relative humidity of near 70%.

## 3. Results

### 3.1. Mean Climate

A progression from homogeneous initial conditions through a period of dominant wave activity and eventually a stationary state, or equilibrated state is illustrated in Figure 2. This figure shows the time evolution of the precipitation rate on the 50M domain. After approximately 20 days of near homogeneous conditions fast, large-amplitude gravity waves as seen in the middle plot develop and propagate through the domain. Approximately 30 days later these waves have been replaced by multiple slowly moving convective systems. Similar waves also occur on other domains but after this early stage no such waves are seen in any of the simulations. The direction of propagation can also occur along either axis, or diagonally. In this later stage the mean values of precipitation, relative humidity, and cloud cover fluctuate about a well defined mean value. It is this mean environmental state represented in Figure 2 (right) which we refer to as the mean equilibrium state, or stationary state, and which is analyzed in this study. All domains show a similar progression from the initial state to equilibrium.

One method of diagnosing whether the atmosphere has reached a statistically stationary state is to examine the time evolution of various quantities. After an initial adjustment period with large fluctuations in the energetics of the simulations stationarity is approached. The evolution of the domain mean total precipitation during the first 2 years of simulation for each of the five domains is shown in Figure 3. Based on the precipitation we judge that all simulations have reached a stationary state after about 200 days, with the 50M and 200M domains adjusting to equilibrium much sooner. Because the 3/4M, 3M, and 12M domains all proceed for longer than 2 years, the average value of the precipitation during the last year of each simulation is shown by the dots at the right of Figure 3, except for the 200M domain for which the last 6 months have been used. This confirms that the mean value has indeed been reached during the period shown. Variations in the precipitation are progressively smaller as the model domain size increases with a

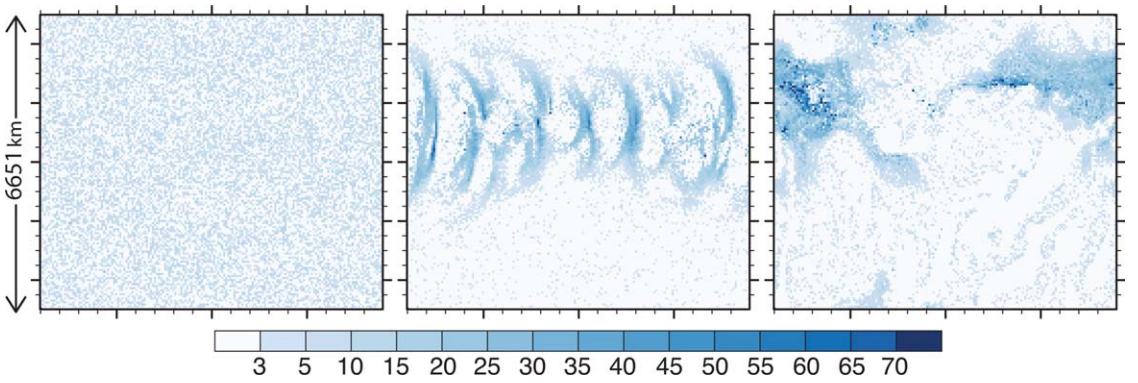


**Figure 2.** Evolution in time of the precipitation rate (mm $d^{-1}$) on the 50M domain with an SST of 301 K. Snapshots are from (left) day 10, (middle) day 25, and (right) day 760. The period of the waves in the middle plot is ≈ 16 h.

convergence of the mean value for the largest domains. The mean (of all domains, with SST=301 K) precipitation is 5 mm $d^{-1}$ with no simulation deviating by more than 7%. The systematic increase in precipitation with domain size is consistent with the systematic decrease of upper level clouds (Figure 5). A decrease in upper level clouds will increase the atmospheric radiative cooling and thus require more convective heating in stationarity.

Basic physical characteristics of the simulated atmospheres can be determined by looking at the domain mean thermodynamic profiles. These are shown for the simulations with SST=297 K in Figure 4. Cloud liquid water, cloud cover, and RH, all maximize in the lowest kilometer. The RH (computed over a liquid surface) drops to its tropospheric minimum value (≈ 15%) at about 7 km. Between roughly 12 km and 16 km there is a maximum of relative humidity, cloud cover, and cloud ice, due to radiatively driven mass convergence in the upper troposphere in clear skies that is satisfied by the detrainment from convective clouds [e.g., *Hartmann and Larson*, 2002; *Zelinka and Hartmann*, 2011]. All domains have three peaks in the cloud cover (0.6 km, 5 km, 13 km), with the upper two cloud maxima corresponding to the melting level clouds and anvil detrainment, respectively. The simulations also uniformly produce two peaks of cloud liquid water below 4km (0.8 km, 2.2 km). Overall, the profiles plausibly represent the mean state of the tropical atmosphere over the oceans and show agreement among all domain sizes on the vertical structure of the atmosphere.

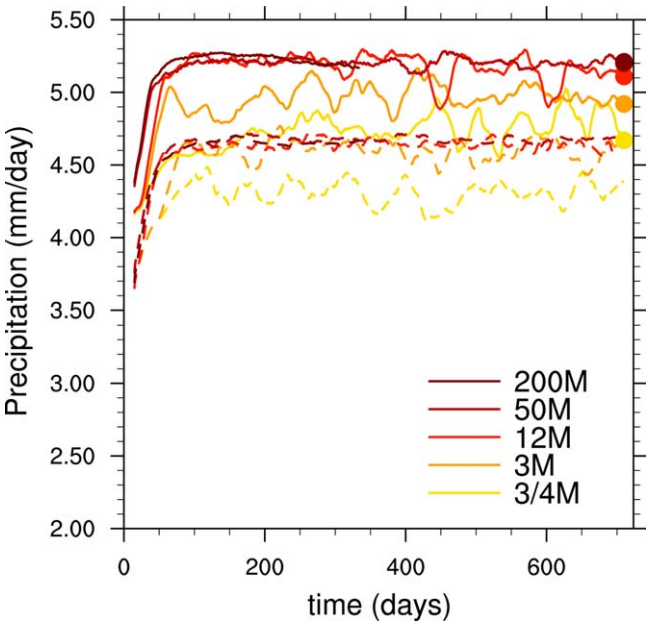


**Figure 3.** Domain mean evolution in time of the total precipitation over the first 2 years of the simulations. Shown is a 30 day running mean. The 200M simulation was run for a total of 1 year and thus only extends through half of the figure. The dots on the right represent the mean total precipitation for the case with an SST of 301K over the last year of each experiment, except for the 200M domain for which the last 6 months have been used. Solid lines represent simulations with an SST of 301 K and dashed lines simulations with an SST of 297 K.

Our simulations are not only coherent across configurations, the vertical structure of the atmospheres is also broadly similar to results found in *Popke et al.* [2013]. Their Figure 4 compares two Global RCE versions of ECHAM6 which differ only by their convection schemes, and one profile from the tropical region of a standard preindustrial control run from the MPI-ESM-LR model. Comparing the profiles from our Figure 4 with Figure 4 from *Popke et al.* [2013] shows that all simulations have a double peak of RH (1 km, 15 km) and a dry

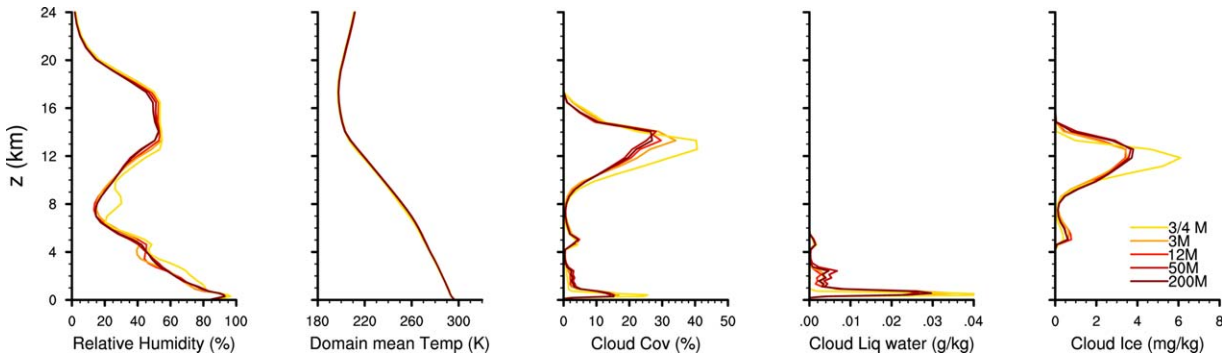


**Figure 4.** Mean vertical profiles with a constant SST of 297 K. Values were computed over the P2 period.

midtroposphere with RH dropping to between 15% and 20% at about 7 km. All simulations have two peaks of cloud cover and cloud liquid water in the lowest 4 km. More importantly, the differences among our domains in Figure 4 are equal to or smaller than the differences between the ECHAM simulations which result from both different physics parameterizations and different SSTs in *Popke et al*. [2013]. Among the profiles from *Popke et al*. [2013] for example, there is a difference of 2–3km in the vertical placement of the RH, cloud fraction, and cloud ice around 15 km. The RH humidity at 15 km differs by up to 20% and one of the temperature profiles is several degrees warmer throughout the troposphere. Considering that ICON and ECHAM differ in dynamical core, physics, resolution, domain and geometry, the similarity of the RCE climates they simulate, both to each other and to the tropical environment of MPI-ESM-LR, points to the broad applicability of the RCE framework.

To give an impression of the relative scale of features present on the 3/4M, 12M, and 200M domains Figure 5 shows the same data as Figure 1, tiled according to scale, periodically repeated to fill a region the size of the 200M domain. The 3/4M, 3M, 12M, and 50M domains all show the precipitation and moisture structures to organize on the largest scale available (Figures 1, 5, and 6). The 200M domain shows signs that the maximum scale of convective organization may be between the 50M and 200M domains, but this deserves further investigation.

The organization of convection into large coherent structures has received much attention over the previous two decades. Several different metrics (subsidence fraction, distance between clusters, bi-modality of water vapor, tropospheric RH, etc. [e.g., *Bretherton et al*., 2005; *Tobin et al*., 2012; *Coppin and Bony*, 2015]) have been used to determine the degree of aggregation in observations or simulations. To provide a quantification of the convective organization the subsidence fraction is computed. This measures the fraction of the model domain with subsiding motion ($w < 0\,\mathrm{m\,s^{-1}}$), typically associated with nonconvective regions. The subsidence fractions for domains 3/4M, 3M, 12M, 50M, and 200M at an SST=297 K (301 K) are 0.72, 0.79, 0.78, 0.76, and 0.77 (0.70, 0.71, 0.75, 0.72, 0.71), respectively. These were computed using the vertical velocity on the model level at approximately 5.5 km (comparable to 500 mb). Histograms of vertical velocity at this level have a peak subsidence of 25 hPa day$^{-1}$ across all domains in good agreement with tropical values given by both *Popke et al*. [2013] and ERA-40 reanalysis [*Bony et al*., 2006]. These subsidence fractions

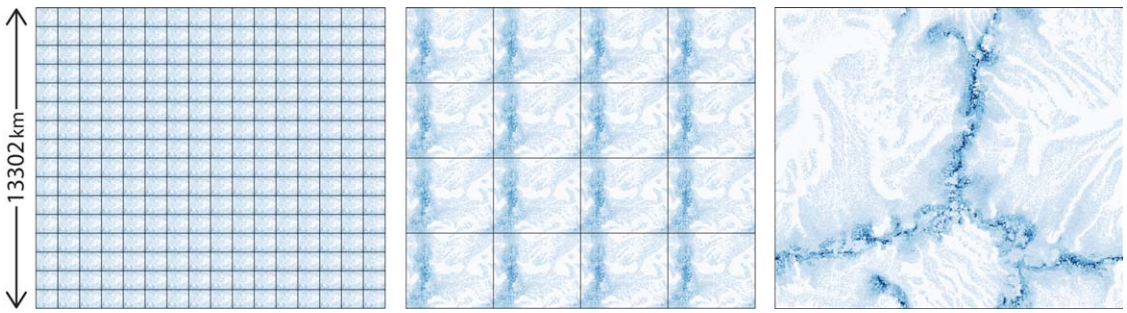


**Figure 5.** Snapshots in time of total precipitation (mm d$^{-1}$) for the (left) 3/4M, (middle) 12M, and (right) 200M domains tiled according to scale. Times and colors are same as for Figure 1, SST=301 K.

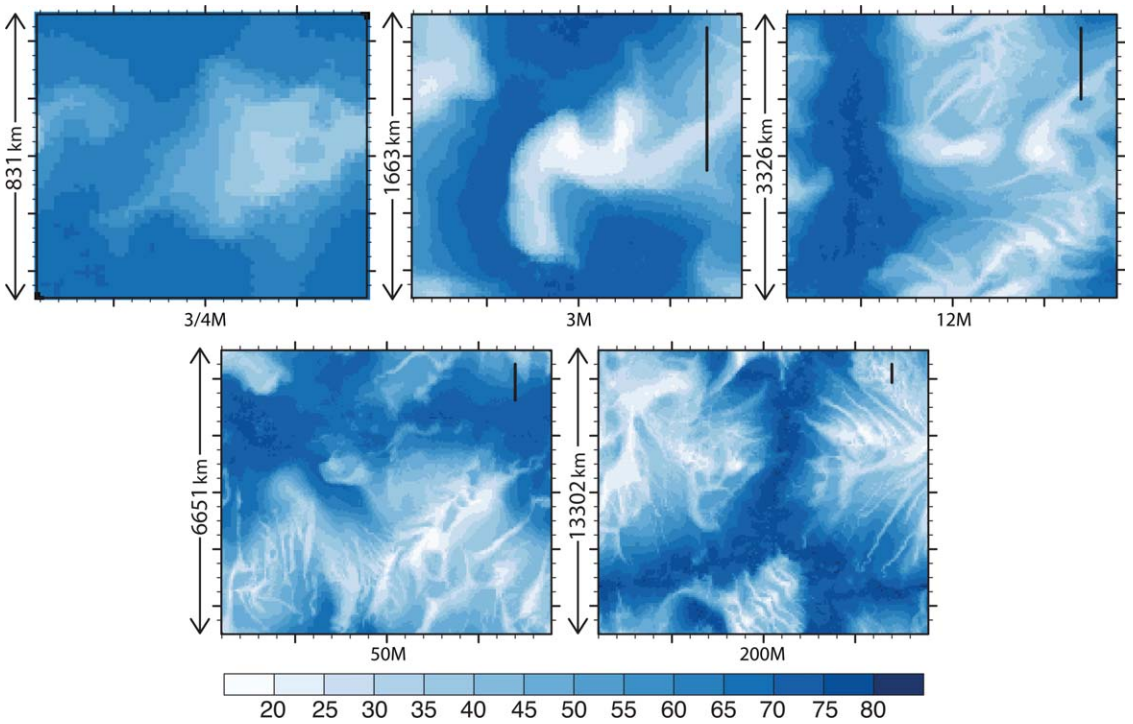


**Figure 6.** Column integrated water vapor (mm). The SST = 301 K and the time of the snapshots is the same as for Figure 1, but the color scale differs. For comparison, the black bar in the 3M, 12M, 50M, and 200M domains represents a length of 830km, corresponding to the short edge length of the 3/4M domain.

are relatively high compared to estimates from reanalysis (0.6) and consistent with an aggregated state, although the structure (Figure 1) is somewhat different from what one typically sees in global [e.g., *Coppin and Bony*, 2015] or cloud resolving [*Bretherton et al.*, 2005] simulations.

The column integrated water vapor for each of the domains is shown in Figure 6, at the same periods of time as seen in Figure 1. This reveals the distribution of the moisture content, even in regions which are not precipitating, and in particular gives a quantitative measure of dry regions. The driest region for the 3/4M domain is relatively moist with 32 mm of vapor in contrast to the largest four domains which have dry regions that drop to about half as much (17 mm) water. Overall the largest four domains show a similar spatial structure of moisture. The filamented structure of the driest regions is intriguing and deserves further study. There is a slight tendency for the difference between the maximum and minimum values of column water vapor to become more pronounced with increasing domain size.

One clear sign of convective aggregation is an abnormally dry mean atmospheric state ($\approx$ 20% RH between 2 and 10 km in *Bretherton et al.* [2005] (Figure 4a, *Tobin et al.*, 2012). This behavior is not pronounced in the present simulations (Figure 5), rather the relative humidity profiles are comparable to the tropical mean profiles of comprehensive GCM simulations. However, the time evolution of the cloud fields and water vapor, the emergent patterns of convection on the largest scales of the domains (Figure 1), the persistence of a few large patches of water vapor (Figure 6), and the consistently high values of the subsidence fraction are consistent with an aggregated state.

Despite the overall similarity of the mean state among the five domains, there are quantitative differences in the mean cloud and ice fields, and the spatial structure of the clouds and water vapor. Column integrated values of the cloud cover, water vapor, cloud liquid water, and cloud ice, as well as the domain mean precipitation are given in Table 2. The differences between domains are most pronounced for the smallest (3/4M) domain. The 3/4M domain does not have the same degree of convective organization as the larger domains and at both 297K and 301K it has the lowest subsidence fraction. The low level peaks of cloud cover and cloud liquid water are larger by about 30% and the cloud ice in the anvil region is larger by 50%. This domain has the lowest mean precipitation (Figure 3 and Table 2), and no secondary peak in cloud liquid water (Figure 4). The total cloud cover, cloud liquid water, and cloud ice of the 3/4M domain also differ

**Table 2.** Total Cloud Cover (Tot CC), Column Integrated Diagnostics (Water Vapor ($\hat{q}_v$), Liquid Water ($\hat{q}_c$), and Ice ($\hat{q}_i$)), and Domain Mean Precipitation (P)[a]

| Domain | SST (K) | Tot CC (%) | $\hat{q}_v$(kg/m$^2$) | $\hat{q}_c$(g/m$^2$) | $\hat{q}_i$(g/m$^2$) | P (mm/d) |
|---|---|---|---|---|---|---|
| 3/4M | 297 | 82 | 39.7 | 15.3 | 6.16 | 4.29 |
| | 301 | 81 | 55.5 | 17.7 | 6.17 | 4.75 |
| 3M | 297 | 73 | 36.4 | 22.2 | 5.03 | 4.60 |
| | 301 | 75 | 52.5 | 25.8 | 5.64 | 4.94 |
| 12M | 297 | 67 | 36.4 | 20.4 | 5.26 | 4.64 |
| | 301 | 63 | 49.7 | 39.3 | 6.35 | 5.19 |
| 50M | 297 | 63 | 37.0 | 24.2 | 5.54 | 4.68 |
| | 301 | 58 | 51.1 | 21.1 | 6.64 | 5.20 |
| 200M | 297 | 64 | 36.9 | 22.5 | 5.60 | 4.65 |
| | 301 | 57 | 51.9 | 26.4 | 6.74 | 5.21 |

[a]Column integrated values are indicated by (ˆ). Values were computed over the P2 period except for precipitation which was computed over the last 6 months for 200M and the last year for all other domains.

(Table 2) from the larger domains. This indicates that despite the relatively large size of the 3/4M domain (960×831 km$^2$) in comparison to previous CRM studies (e.g., *Bretherton et al*. [2005] used a domain of 576×576 km$^2$ and *Wing and Emanuel* [2014] a domain of 768×768 km$^2$), the 3/4M domain is not sufficiently large enough to simulate an atmospheric state that is physically consistent with that of the larger domains. Overall, the vertical thermodynamic profiles and the time evolution of precipitation show convergence toward a common structure as the domain size increases with the 50M and 200M domains appearing practically indistinguishable.

### 3.2. Sensitivity to Sea-Surface Temperature

Here we examine the response of the RCE simulations to a uniform SST perturbation of 4 K. The difference between the domain mean profiles for the two sets of simulations is shown in Figure 7. The basic behavior and mean vertical structure of the simulations with an SST of 297 K is qualitatively similar to those with an SST of 301 K. As with the mean state discussed in the previous section, as the domain size increases the spread of the response among the simulations converge toward a common structure with a particularly strong overlap in the cloud cover, cloud liquid water, and cloud ice between 50M and 200M. At higher SSTs the specific humidity increases and temperature warms throughout the atmosphere for all domains with the maximum warming occurring at 13–14 km. While the magnitudes differ, the maximum and minimum of cloud cover, cloud ice, cloud liquid water, and temperature occur at similar levels among the domains.

Cloud cover, cloud ice, and RH all exhibit a spatial dipole of positive and negative values between 10 and 20 km that can be explained by a vertical shift of the profiles as the surface warms (Figure 7). For example, the height of the maximum cloud cover from convective anvil detrainment shifts from 12–14 km to 14–16 km. This shift of upper level clouds is shown as a function of temperature in Figure 8. For each of the different surface temperatures, the temperature of the maximum upper level cloud is approximately independent of domain. According to the Fixed Anvil Temperature (FAT) hypothesis, as the surface warms the upper level clouds shift vertically with a constant anvil cloud top temperature [*Hartmann and Larson*, 2002].

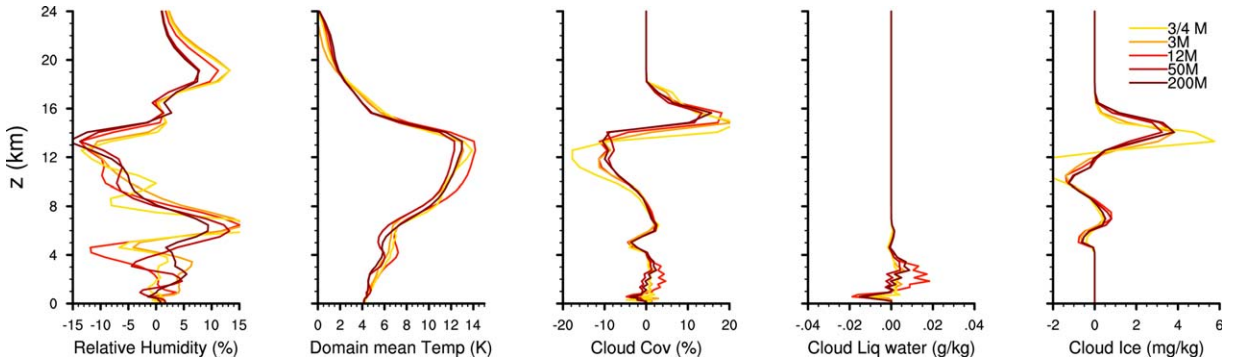


**Figure 7.** Response of simulations to warming shown as the difference (301K−297K) of mean vertical profiles between the two sets of fixed SST cases. Values were computed over the P2 period.

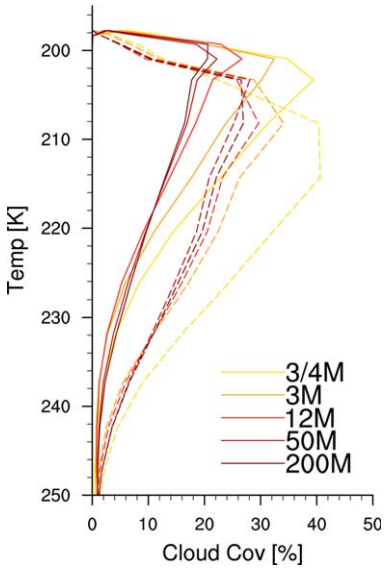


**Figure 8.** Response of upper level cloud cover to warming plotted on temperature levels. Simulations with SST = 301K shown by solid lines, and SST = 297K by dashed lines. Values were computed over the P2 period.

The upper level clouds in Figure 8 do not shift vertically isothermally, but the change in the temperature of the upper level clouds ($\approx -5$K) is less than half of the temperature increase ($\approx$ 15K) on a constant height level.

There is variation between individual simulations in the response of the RH, but for all simulations the RH shifts vertically with warming resulting in consistent increases of RH above 15 km and between 5 and 8 km, and drying between 8 and 15 km. The RH difference profiles of all domains have fluctuations on the order of 15% with roughly the same vertical levels of tropospheric maxima and minima and nonsystematic fluctuations above about 0.6 km. The cloud layer at the melting level shifts uniformly for all domains from a height of 5 km when the SST is 297 K to between 6 and 7 km in the case with a warmer SST.

Between the surface and about 5 km the response seen in Figure 7 indicates a nontrivial interaction of changing surface fluxes, cloud cover, and turbulent mixing. A number of studies have argued that the response of tropical low clouds to warming is decisive for the determination of the cloud feedbacks. It has been hypothesized that as SSTs rise, enhanced mixing of the boundary layer air with the drier free troposphere dries out the cloud layer and results in less clouds [e.g., *Rieck et al*., 2012]. *Brient et al*. [2016] showed that models with a pronounced maximum in low cloud amount at cloud base are most susceptible to convective drying, but not through a reduction of clouds throughout the cloud layer, as shown by *Rieck et al*. [2012], rather by a reduction of cloud amount at cloud base. This effect is pronounced in our simulations, and is robust as it appears irrespective of the domain size.

All domains show a pronounced cloud base peak in liquid water, which is systematically reduced as the surface temperature increases. To highlight the response of the moisture content in the boundary layer Figure 9 shows the RH, cloud cover, and cloud liquid water from Figure 7, along with specific humidity (qv), focused only on the lowest 4 km. Although the domains with an SST of 301 K have higher specific humidity and RH in the lowest 0.6 km, the cloud liquid water and cloud cover (except for 3M) decrease there. The increase of RH below 0.6 km can be understood as a consequence of the energetics for a tropical system of RCE. Relative humidity in the planetary boundary layer should increase when the convective mass flux decreases

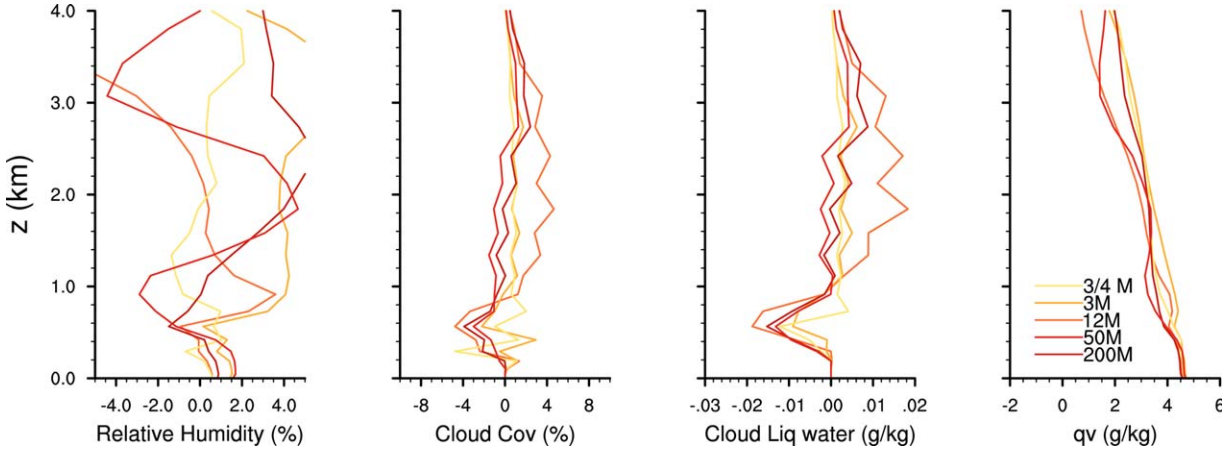


**Figure 9.** Same data as Figure 7, zoomed in to reveal boundary layer features. Values were computed over the P2 period.

[see *Satoh*, 2013, equation (15.4.11)]. The decrease of the convective mass flux in a warming atmosphere follows from the approximation that $M_c \propto P/q$, where $M_c$ is the convective mass flux, $P$ is the precipitation, and $q$ is the mixing ratio of water vapor [*Betts and Ridgway*, 1989; *Held and Soden*, 2006]. As the surface temperature warms, $P$ will increase at a slower rate than $q$, implying a decrease of $M_c$. The change of $P$ and the changes of water vapor (Tables 2 and 3) confirm that $M_c$ should decrease for our simulations, and thus that boundary layer RH should increase with warming.

Between the surface and 0.6 km, the change of RH, cloud liquid water, and specific humidity decrease with height for all domains. A decrease of cloud cover and cloud liquid water in the BL could indicate a deepening BL with dry tropospheric air being entrained from above. However, the total response of low clouds to warming in GCMs results from a balance between drying from the convective parameterization and moistening by the turbulence parameterization. Different balances between these processes were argued [*Brient et al*., 2016; *Sherwood et al*., 2014] to be one of the primary factors leading to the spread of total feedback in CMIP models. All of our simulations show (Figure 9) a uniform decrease of cloud liquid water (0.6 km) and a decrease with height of low-level water vapor in response to warming but the response of cloud cover and RH is not systematic across domains. The implications of this on the feedback parameter will be discussed in the next section.

The partition between convective and large-scale precipitation is likely to influence a model's climate response to warming [*Held et al*., 2007]. In the present simulations the parameterized convection scheme accounts for almost all (about 90%) of the precipitation. Domains with warmer SSTs have less convective precipitation. The fraction of convective precipitation for domains 3/4M, 3M, 12M, 50M, and 200M at an SST=301 K (297 K) are 0.94, 0.89, 0.82, 0.88, and 0.88 (0.95, 0.89, 0.90, 0.92, 0.92), respectively. A clear connection between the partitioning of precipitation types and the feedbacks is not obvious.

### 3.3. Climate Change Feedbacks and Hydrologic Cycle Sensitivity

To estimate the climate feedback parameter, $\lambda$, the difference between the top-of-atmosphere radiance in the warm simulation and the cooler simulation is normalized by the SST difference, e.g., following *Cess et al*. [1989]. Given the climate feedback parameter the equilibrium climate sensitivity can be estimated as $-F_{2\times CO_2}/\lambda$, for which purpose we adopt a value of $F_{2\times CO_2}=3.7\,\mathrm{Wm}^{-2}$ following *Myhre et al*. [1998]. The reader is referred to *Sherwood et al*. [2015], for a broader discussion of forcing and feedback concepts. This method is arguably the most direct method for estimating the climate feedback parameter. The hydrological sensitivity parameter can similarly be defined [e.g., *Fläschner et al*., 2016] as the slope of temperature-dependent precipitation change ($\Delta P/\Delta T$).

The thus calculated feedback parameters, climate- and hydrologic sensitivities of our simulations vary with domain size (Table 3) in a nonsystematic fashion. Variations in the climate feedback parameter are large, (1.8 $\pm$0.5), and differ by a factor of about two between the largest and smallest value. In contrast, variations in the hydrological sensitivity parameter are much smaller, (2.4 $\pm$0.3), and vary by a factor of 1.4. Relative contributions from the long- and shortwave components of the total feedback parameter are also tabulated. Although the magnitude of the longwave feedback parameters are larger, the range of the shortwave feedback parameters ($2.6\,\mathrm{Wm}^{-2}\mathrm{K}^{-1}$) is greater than those of the longwave feedback parameters ($1.35\,\mathrm{Wm}^{-2}\mathrm{K}^{-1}$). The shortwave feedback contributes the most to the variability of the total feedback response, but it is clear that the contribution of the longwave component cannot be neglected for either the climate feedback parameter or the hydrologic sensitivity parameter. This likely

**Table 3.** Mean Energetics[a]

| Domain | $\lambda_{sw}/\lambda_{sw,clr}\,(\mathrm{W/m^2K})$ | $\lambda_{lw}/\lambda_{lw,clr}\,(\mathrm{W/m^2K})$ | $\lambda\,(\mathrm{W/m^2K})$ | ECS (K) | HSP (%/K) |
|---|---|---|---|---|---|
| 0.75 M | 0.08/0.25 | −1.93/−2.13 | −1.85 $\pm$(0.5/0.4) | 2.00 | 2.3 |
| 3M | −0.89/0.25 | −1.49/−1.55 | −2.39 $\pm$(0.4/0.3) | 1.55 | 1.9 |
| 12M | 0.13/0.23 | −2.28/−2.48 | −2.15 $\pm$(0.4/0.3) | 1.72 | 2.6 |
| 50M | 1.71/0.25 | −2.84/−2.05 | −1.13 $\pm$(0.2/0.2) | 3.29 | 2.7 |
| 200M | 0.92/0.25 | −2.51/−2.25 | −1.59 $\pm$(0.2/0.2) | 2.33 | 2.7 |

[a]Long- and short-wave feedback parameters, total feedback parameter, equilibrium climate sensitivity (ECS) and hydrologic sensitivity parameter (HSP) (defined as $\Delta P/\Delta T_s$, where $P$ is the total precipitation) as a function of domain size. Values were averaged over the P1 period.

indicates an interplay of multiple mechanisms in the response. As is to be expected, the hydrological sensitivity scales closely with the change in atmospheric cooling (not shown) which is dominated by longwave feedbacks, (i.e., not variability in atmospheric shortwave absorption as is evident when looking across climate models [e.g., *Takahashi*, 2009])) and thus the weakest sensitivity is found in the 3M domain.

The Cloud Radiative Effect (CRE = clear-sky radiance - all-sky radiance) can be used to investigate the role of clouds in the response to a perturbation. We find that variation in shortwave feedbacks is dominated by cloud radiative effects (Table 3) as the clear-sky shortwave feedback is practically domain-size independent, whereas in the longwave both cloud and clear-sky feedbacks are important. The spread of the longwave clear-sky (temperature plus water vapor) feedback is larger than expected. This could be influenced by the amount of water vapor in clear-sky regions, the partition between convective and large-scale precipitation, and the degree to which the clouds of a simulation are aggregated. There is also a nonsystematic variation of the low-level RH response to warming that could be important (Figure 9). Computing the change of CRE ($\Delta$CRE) between the simulations with different SSTs and decomposing this into the shortwave and longwave components reveals that the shortwave $\Delta$CRE varies in sync with the total $\Delta$CRE while the longwave $\Delta$CRE is approximately independent of domain size.

The variation in shortwave cloud feedback and $\Delta$CRE across the domain sizes is difficult to ascribe to specific features of the mean state or response. While the nonsystematic response of the low clouds strongly contributes to this variation, other factors also contribute. All domains have an increase of upper level clouds between 14 and 18km with the differences in magnitude (up to 5%) contributing to differences in the longwave feedback parameters shown in Table 3. Although the response of upper level clouds is broadly consistent across domains (Figure 8), the varying degree to which each domain satisfies the proportionately higher anvil temperature hypothesis may contribute to the spread of the longwave feedback [*Zelinka and Hartmann*, 2010]. We also see (Figure 9) that the response of the low-level specific and relative humidity differs slightly from the cloud cover response indicating the importance of surface fluxes and turbulent mixing.

Considering the only difference among the simulations is the size of the domain, and the similarity of the thermodynamic response (Figure 7), the substantial spread in the feedback parameters is surprising. Despite having identical physics parameterizations, the range of feedback parameters that we calculate (1.3 $Wm^{-2}K^{-1}$) is larger than the range from the models which participated in CMIP5 (1.1 $Wm^{-2}K^{-1}$). To illustrate this the feedback parameters for each domain size are shown in Figure 10. The values for individual models from CMIP5 are also displayed with the black markers. These results highlight the ability of different simulations to have similar climates but differing climate sensitivities [*Mauritsen et al.*, 2012; *Zhao et al.*, 2016].

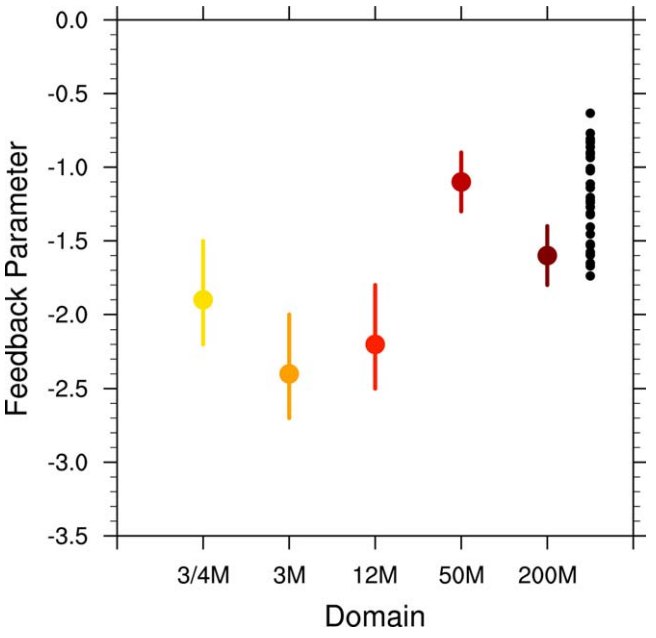


**Figure 10.** Feedback parameter ($Wm^{-2}K^{-1}$) as a function of domain size. Bars correspond to a 97.5% confidence interval with a one-sided t-test. A de-correlation time of three weeks was assumed for all domains. The feedback parameters from CMIP5 models are shown by the black markers.

## 4. Conclusions

It has been shown that the simulated atmosphere of the ICON GCM run into RCE is sufficiently similar across a range of domain sizes to justify and encourage the use of RCE to study both a GCM and a CRM on the same domain with the goal of improved constraints

on the parameterized clouds. This was demonstrated with SST perturbation simulations on multiple domains in a state of RCE. The equilibrated stationary states of the largest four domains have nearly indistinguishable thermodynamic profiles while the smallest domain, 3/4M, differs with less precipitation, more cloud ice, and larger values of cloud cover. In addition to these differences, the 3/4 M domain has the lowest subsidence fraction. As a result the 3/4 M domain appears to be too small for the RCE studies recommended by this study. However, for all simulations the low-level RH, cloud cover, and cloud liquid water maximize below 1km. All simulations have a peak in cloud cover at the melting level of the same magnitude and the upper level cloud ice, cloud cover, and RH indicate that the vertical extent of convection is similar for all domains. There is a systematic increase of the domain mean precipitation as a function of domain size for the smaller domains but convergence has been reached in the largest three domains. Overall, the resulting model state resembles that of the tropical atmosphere on Earth.

Notwithstanding the qualitative similarities of the simulations, quantitative differences lead to a surprisingly large sensitivity of the feedback parameter, and thus the climate sensitivity, on domain size. The range of the feedback parameter (1.3 $Wm^{-2}K^{-1}$) is more than a factor of two and is comparable to the range of feedbacks which were obtained by the CMIP5 models (1.1 $Wm^{-2}K^{-1}$, Figure 10). Due to our experimental setup the different values of the feedback parameter in these simulations cannot be due to differences in the subgrid scale parameterization schemes, grid, discretization, or formulations of the dynamical core. Among the remaining possible factors it seems likely that some combination of nonlinear interactions between the wind field, surface fluxes, low-level clouds, and radiation are responsible for the variations in the feedback. We interpret these changes as a possible manifestation of structural instability [*McWilliams*, 2007] that has been hypothesized to exist in some models, and may also be a characteristic of the natural system.

These results offer encouragement for future tests on regional domains using models with both explicit and parameterized convection. Despite its apparent imprecision with regard to the feedback parameter, the paradigm of RCE is a compelling simplification of the atmosphere that is interesting to study, not only for its well appreciated insight into quantities like climate sensitivity, but more fundamentally because of its ability to elucidate the ways in which convection and large-scale circulations interact.

**Acknowledgments**

The authors thank Timothy W. Cronin and an anonymous reviewer for instructive feedback that clarified the manuscript. Anurag Dipankar and Leonidas Linardakis assisted with debugging and stimulating discussions. Cathy Hohenegger read an early version of the manuscript and helped to improve the presentation of our ideas. The computing resources were provided by Deutsches Klimarechenzentrum (DKRZ). The research presented here was conducted when LGS was employed by the Max Planck Institute for Meteorology. The ICON development team at both MPI-M and DWD provided helpful support and motivation throughout the work. Primary data and scripts used in the analysis have been archived by the Max Planck Institute for Meteorology and can be obtained by contacting publications@mpimet.mpg.de. Princeton University generously supported LGS during the final stage of the writing. LGS thanks Catherine Raphael for assistance with Figures 1–5, and 6.

## References

Arnold, N. P., and D. A. Randall (2015), Global-scale convective aggregation: Implications for the Madden-Julian Oscillation, *J. Adv. Model. Earth Syst.*, *7*, 1499–1518, doi:10.1002/2015MS000498.

Bechtold, P., E. Bazile, F. Guichard, P. Mascart, and E. Richard (2001), A mass-flux convection scheme for regional and global models, *Q. J. R. Meteorol. Soc.*, *127*, 869–886, doi:10.1002/qj.49712757309.

Bechtold, P., M. Köhler, T. Jung, F. Doblas-Reyes, M. Leutbecher, M. J. Rodwell, F. Vitart, and G. Balsamo (2008), Advances in simulating atmospheric variability with the ECMWF model: From synoptic to decadal time-scales, *Q. J. R. Meteorol. Soc.*, *134*, 1337–1351, doi:10.1002/qj.289.

Bechtold, P., N. Semane, P. Lopez, J.-P. Chaboureau, A. Beljaars, and N. Bormann (2014), Representing equilibrium and nonequilibrium convection in large-scale models, *J. Atmos. Sci.*, *71*, 734–753, doi:10.1175/JAS-D-13-0163.1.

Becker, T., and B. Stevens (2014), Climate and climate sensitivity to changing $CO_2$ on an idealized land planet, *J. Adv. Model. Earth Syst.*, *6*, 1205–1223, doi:10.1002/2014MS000369.

Betts, A., and W. Ridgway (1989), Climatic equilibrium of the atmospheric convective boundary layer over a tropical ocean, *J. Atmos. Sci.*, *46*, 2621–2641, doi:10.1175/1520-0469(1989)046¡2621:CEOTAC¿2.0.CO;2.

Bony, S., and J. L. Dufresne (2005), Marine boundary layer clouds at the heart of tropical cloud feedback uncertainties in climate models, *Geophys. Res. Lett.*, *32*, L20806, doi:10.1029/2005GL023851.

Bony, S., et al. (2006), How well do we understand and evaluate climate change feedback processes?, *J. Clim.*, *19*, 3445–3482, doi:10.1175/JCLI3819.1.

Bony, S., et al. (2015), Clouds, circulation, and climate sensitivity, *Nat. Geosci.*, *8*, 261–268, doi:10.1038/NGEO2398.

Bretherton, C. S., P. N. Blossey, and M. Khairoutdinov (2005), An energy-balance analysis of deep convective self-aggregation above uniform SST, *J. Atmos. Sci.*, *62*, 4273–4292.

Brient, F., T. Schneider, Z. Tan, S. Bony, X. Qu, and A. Hall (2016), Shallowness of tropical low clouds as a predictor of climate models' response to warming, *Clim. Dyn.*, *47*, 433–449, doi:10.1007/s00382-015-2846-0.

Cess, R. D., G. L. Potter, and J. Blanchet (1989), Interpretation of cloud-climate feedback as produced by 14 atmospheric general circulation models, *Science*, *245*, 513–516.

Coppin, D., and S. Bony (2015), Physical mechanisms controlling the initiation of convective self-aggregation in a general circulation model, *J. Adv. Model. Earth Syst.*, *7*, 2060–2078, doi:10.1002/2015MS000571.

Derbyshire, S. H., I. Beau, P. Bechtold, J.-Y. Grandpeix, J.-M. Piriou, J.-L. Redelsperger, and P. Soares (2004), Sensitivity of moist convection to environmental humidity, *Q. J. R. Meteorol. Soc.*, *130*, 3055–3079.

Dipankar, A., B. Stevens, R. Heinze, C. Moseley, G. Zängl, M. Giorgetta, and S. Brdar (2015), Large eddy simulation using the general circulation model ICON, *J. Adv. Model. Earth Syst.*, *7*, 963–986, doi:10.1002/2015MS000431.

Emanuel, K., A. A. Wing, and E. M. Vincent (2014), Radiative-convective instability, *J. Adv. Model. Earth Syst.*, *6*, 75–90, doi:10.1002/2013MS000270.

Fläschner, D., T. Mauritsen, and B. Stevens (2016), Understanding the intermodel spread in global-mean hydrological sensitivity, *J. Clim.*, *29*, 801–817, doi:10.1175/JCLI-D-15-0351.1.
Gassmann, A. (2011), Inspection of hexagonal and triangular c-grid discretizations on the shallow water equations, *J. Comput. Phys.*, *230*, 2706–2721, doi:10.1002/2013MS000270.
Hartmann, D. L., and K. Larson (2002), An important constraint on tropical cloud-climate feedback, *Geophys. Res. Lett.*, *29*(20), 1951, doi:10.1029/2002GL015835.
Held, I. M., and B. J. Soden (2006), Robust responses of the hydrologic cycle to global warming, *J. Clim.*, *19*, 5686–5699, doi:10.1175/JCLI3990.1.
Held, I. M., R. S. Hemler, and V. Ramaswamy (1993), Radiative-convective equilibrium with explicit two-dimensional moist convection, *J. Atmos. Sci.*, *50*, 3909–3927, doi:10.1175/1520-0469(1993)050¡3909:RCEWET¿2.0.CO;2.
Held, I. M., M. Zhao, and B. Wyman (2007), Dynamic radiative-convective equilibria using GCM column physics, *J. Atmos. Sci.*, *64*, 228–238, doi:10.1175/JAS3825.11.
Jeevanjee, N., and D. M. Romps (2013), Convective self-aggregation, cold pools, and domain size, *Geophys. Res. Lett.*, *40*, 994–998, doi:10.1002/grl.50204.
Klemp, J. B., J. Dudhia, and A. D. Hassiotis (2008), An upper gravity-wave absorbing layer for NWP applications, *Mon. Weather Rev.*, *136*, 3987–4004, doi:10.1175/2008MWR2596.1.
Manabe, S., and R. F. Strickler (1964), Thermal equilibrium of the atmosphere with a convective adjustment, *J. Atmos. Sci.*, *21*, 361–385.
Manabe, S., and R. T. Wetherald (1967), Thermal equilibrium of the atmosphere with a given distribution of relative humidity, *J. Atmos. Sci.*, *24*, 241–259.
Mauritsen, T., and B. Stevens (2015), Missing iris-effect as a possible cause of muted hydrological change and high climate sensitivity in models, *Nat. Geosci.*, *8*, 346–351.
Mauritsen, T., et al. (2012), Tuning the climate of a global model, *J. Adv. Model. Earth Syst.*, *4*, M00A01, doi:10.1029/2012MS000154.
McWilliams, J. C. (2007), Irreducible imprecision in atmospheric and oceanic simulations, *Proc. Natl. Acad. Sci. U. S. A.*, *104*, 8709–8713, doi:10.1073/pnas.0702971104.
Mlawer, E. J., S. J. Taubman, P. D. Brown, M. J. Iacono, and S. A. Clough (1997), Radiative transfer for inhomogeneous atmospheres: RRTM, a validated correlated-k model for the longwave, *J. Geophys. Res.*, *102*, 16,663–16,682.
Muller, C. J., and I. Held (2012), Detailed investigation of the self-aggregation of convection in cloud-resolving simulations, *J. Atmos. Sci.*, *69*, 2551–2565, doi:10.1175/JAS-D-11-0257.1.
Myhre, G., E. J. Highwood, K. P. Shine, and F. Stordal (1998), New estimates of radiative forcing due to well mixed greenhouse gases, *Geophys. Res. Lett.*, *25*, 2715–2718.
Nakajima, K., and T. Matsuno (1988), Numerical experiments concerning the origin of cloud clusters in the tropical atmosphere, *J. Meteorol. Soc. Jpn.*, *66*, 309–329.
Nam, C., S. Bony, J.-L. Dufresne, and H. Chepfer (2012), The 'too few, too bright' tropical low-cloud problem in CMIP5 models, *Geophys. Res. Lett*, *39*, L21801, doi:10.1029/2012GL053421.
Nuijens, L., B. Medeiros, I. Sandu, and M. Ahlgrimm (2015), The behavior of trade-wind cloudiness in observations and models: The major cloud components and their variability, *J. Adv. Model. Earth Syst.*, *7*, 600–616, doi:10.1002/2014MS000390.
Popke, D., B. Stevens, and A. Voigt (2013), Climate and climate change in a radiative-convective equilibrium version of ECHAM6, *J. Adv. Model. Earth Syst.*, *5*, 1–14, doi:10.1029/2012MS000191.
Raschendorfer, M. (2001), The new turbulence parameterization of LM, *COSMO Newsl.*, *1*, 89–97. [Available at http://www.cosmo-model.org.]
Redelsperger, J., D. Parsons, and F. Guichard (2002), Recovery process and factors limiting cloud-top height following the arrival of a dry intrusion observed during TOGA-COARE, *J. Atmos. Sci.*, *59*, 2438–2457.
Reed, K. A., B. Medeiros, J. T. Bacmeister, and P. H. Lauritzen (2015), Global radiative-convective equilibrium in the Community Atmosphere Model, version 5, *J. Atmos. Sci.*, *72*, 2183–2197, doi:10.1175/JAS-D-14-0268.1.
Rieck, M., L. Nuijens, and B. Stevens (2012), Marine boundary layer cloud feedbacks in a constant relative humidity atmosphere, *J. Atmos. Sci.*, *69*, 2538–2550, doi:10.1175/JAS-D-11-0203.1.
Rio, C., F. Hourdin, J.-Y. Grandpeix, and J.-P. Lafore (2009), Shifting the diurnal cycle of parameterized deep convection over land, *Geophys. Res. Lett*, *36*, doi:10.1029/2008GL036799.
Satoh, M. (2013), *Atmospheric Circulation Dynamics and General Circulation Models*, 2nd ed., 756 pp., Springer-PRAXIS, N. Y.
Seifert, A. (2008), A revised cloud microphysical parameterization for COSMO-LME, *COSMO Newsl.*, *8*, 25–28. [Available at http://www.cosmo-model.org.]
Sherwood, S. C., S. Bony, and J. L. Dufresne (2014), Spread in model climate sensitivity traced to atmospheric convective mixing, *Nature*, *505*, 37–42, doi:10.1038/nature12829.
Sherwood, S. C., S. Bony, O. Boucher, C. Bretherton, P. M. Forster, J. M. Gregory, and B. Stevens (2015), Adjustments in the forcing-feedback framework for understanding climate change, *Bull. Am. Meteorol. Soc.*, *96*, 217–228, doi:10.1175/BAMS-D-13-00167.1.
Sommeria, G., and J. W. Deardorff (1977), Subgrid-scale condensation in models of nonprecipitating clouds, *J. Atmos. Sci.*, *34*, 344–355, doi:10.1175/1520-0469(1977)034¡0344:SSCIMO¿2.0.CO;2.
Stevens, B., and S. Bony (2013), What are climate models missing?, *Science*, *340*, 1053–1054, doi:10.1126/science.1237554.
Stevens, B., et al. (2013), Atmospheric component of the MPI-M earth system model: ECHAM6, *J. Adv. Model. Earth Syst.*, *5*, 146–172, doi:10.1002/jame.20015.
Sundqvist, H. (1978), A parameterization scheme for non-convective condensation including prediction of cloud water content, *Q. J. R. Meteorol. Soc.*, *104*, 677–690, doi:10.1002/qj.49710444110.
Takahashi, K. (2009), The global hydrological cycle and atmospheric shortwave absorption in climate models under $CO_2$ forcing, *J. Clim.*, *22*, 5667–5675.
Tobin, I., S. Bony, and R. Roca (2012), Observational evidence for relationships between the degree of aggregation of deep convection, water vapor, surface fluxes, and radiation, *J. Clim.*, *25*, 6885–6904.
Tompkins, A., and G. Craig (1998), Radiative-convective equilibrium in a three-dimensional cloud ensemble model, *Q. J. R. Meteorol. Soc.*, *124*, 2073–2097.
Wan, H., et al. (2013), The ICON-1.2 hydrostatic atmospheric dynamical core on triangular grids––Part 1: Formulation and performance of the baseline version, *Geosci. Model Dev.*, *6*, 735–763, doi:10.5194/gmd-6-735-2013.
Webb, M., C. Senior, S. Bony, and J.-L. Morcrette (2001), Combining ERBE and ISCCP data to assess clouds in the hadley centre, ECMWF and LMD atmospheric climate models, *Clim. Dyn.*, *17*, 905–922.

Wing, A. A., and T. W. Cronin (2016), Self-aggregation of convection in long channel geometry, *Q. J. R. Meteorol. Soc.*, *142*, 1–15, doi: 10.1002/qj.2628.

Wing, A. A., and K. A. Emanuel (2014), Physical mechanisms controlling self-aggregation of convection in idealized numerical modeling simulations, *J. Adv. Model. Earth Syst.*, *6*, 59–74, doi:10.1002/2013MS000269.

Zängl, G., D. Reinert, P. Ripodas, and M. Baldauf (2015), The ICON(ICOsahedral Non-hydrostatic modelling framework of DWD and MPI-M: Description of the non-hydrostatic dynamical core), *Q. J. R. Meteorol. Soc.*, *141*, 563–579, doi:10.1002/qj.2378.

Zelinka, M. D., and D. L. Hartmann (2010), Why is longwave cloud feedback positive?, *J. Geophys. Res.*, *115*, D16117, doi:10.1029/2010JD013817.

Zelinka, M. D., and D. L. Hartmann (2011), The observed sensitivity of high clouds to mean surface temperature anomalies in the tropics, *J. Geophys. Res.*, *116*, D23103, doi:10.1029/2011JD016459.

Zhao, M., et al. (2016), Uncertainty in model climate sensitivity traced to representations of cumulus precipitation microphysics, *J. Clim.*, *29*, 543–560.

Zhou, W. (2015), Non-rotating and rotating raditive-convective equilibrium, PhD thesis, Program in Atmos. and Oceanic Sci., Dept. of Geosci., Princeton Univ, Princeton, New Jersey.